Nanoemulsion Composite Microgels for Orthogonal Encapsulation and Release

*Harry Z. An, Matthew E. Helgeson, and Patrick S. Doyle**

Polymer hydrogels and microgels have been widely exploited for the controlled storage, delivery and detection of active compounds, including small molecules and biologics.[1,2] However, due to their intrinsically hydrated microenvironment, the development of hydrogels for encapsulation and/or release of poorly water-soluble cargos remains a persistent challenge.[3] As such, the development of novel hydrogels with well-controlled hydrophobic compartments remains important to a number of delivery applications including pharmaceuticals,[3,4] cosmetics,[5] foods,[6] imaging,[7] and sensors.[8] Recent strategies to overcome this challenge include modification of the hydrogel polymer network by co-polymerizing or grafting hydrophobic units to create hydrophobic domains within the polymer matrix, thereby increasing solubility of poorly-soluble actives,[9] or by direct conjugation of such actives to the polymer itself.[10] However, these approaches are limited by relatively low loading capacities and the need for designer polymers.[3] An alternative approach is to incorporate hydrophobic colloidal species into the hydrogel matrix, including nanoparticles,[11–13] vesicles,[14] micelles,[15] emulsions[16] and microemulsions.[17] Although such hydrogel composites have shown some success, material systems that can simultaneously achieve high loading and tunable release for a range of poorly-soluble actives are lacking.[7]

Recently, we have demonstrated the formation of crosslinkable nanoemulsions with controlled droplet size, loading, and stability in which nanoscale oil droplets are suspended in a hydrogel pre-cursor.[18] The encapsulation of nanoemulsions within a hydrogel matrix affords these materials several advantages compared with other advanced materials for encapsulation of hydrophobic compounds. The ability to produce nanoemulsions at high volume fractions allows for precise control of loading within the hydrogel, while the ability to tune the hydrogel network allows for a controlled barrier to release.[3,19] Compared to ordinary emulsions, nanoemulsions also exhibit increased surface-to-volume ratio, which enhances release kinetics and bioavailability, and greater kinetic stability, which improves shelf life.[19] Furthermore, the inherent control and homogeneity of droplet properties such as their size[20] distinguishes them from polymeric micellar[21] and vesicular[22] cargos, which are inherently polydisperse and can be adversely affected by a polymer matrix.[23]

In previous work, we tested the ability to process crosslinkable nanoemulsions using flow lithography (FL) for the synthesis of structured composite microgel particles.[18] Flow lithography[24,25] has been used to generate microgels with sophisticated architecture, including shape and chemical anisotropy,[26,27] and tunable diffusion[28] and degradation[29] profiles. As such, the potential to combine crosslinkable nanoemulsions with flow lithography can provide particle-based delivery vehicles with homogeneous nano-scale distribution of hydrophobic compartments, while at the same time allowing their spatial localization within the hydrogel matrix, a combination which is lacking in other fluidic-based approaches.[30–34] Here, we extend the previous studies to explore novel motifs for multi-platform encapsulation and delivery of active compounds from nanoemulsion composite microgels. In doing so, we demonstrate several orthogonal methods by which both hydrophobic and hydrophilic compounds, including small molecules, proteins and the nanoemulsion droplets themselves, can be effectively encapsulated in and released from the resulting microparticles.

To synthesize nanoemulsion composite microgels, we use "oil-in-pregel" (O/PG) nanoemulsions containing low molecular weight silicone oil droplets stabilized by sodium dodecyl sulfate (SDS), dispersed in an aqueous gel pre-cursor containing poly(ethylene glycol) diacrylate (PEGDA) monomer and photoinitiator (Darocur 1173). Photopolymerization of the O/PG nanoemulsion results in the formation of a chemically crosslinked hydrogel in the continuous phase. The O/PG nanoemulsions are produced by high pressure homogenization,[20] and can be readily prepared across a range of droplet sizes and continuous phase compositions.[18] Once formed, the nano-scale nature of the resulting emulsion droplets ($D <$ 100 nm) provides the optical transparency essential for photopatterning (**Figure 1**A), whereas larger droplets inhibit FL due to light scattering.[18] The canonical photopolymerizable nanoemulsion formulation used for particle synthesis shown in this work contains droplet volume fraction $\varphi = 0.20$, although emulsion loadings up to $\varphi = 0.33$ gave similar results (see Supporting Information).

The O/PG nanoemulsions were used as the process fluid for stop-flow lithography (SFL)[24,25] to create shape-anisotropic microgels with a variety of extruded shapes (Figure 1B). To demonstrate successful encapsulation of the nanoemulsion within the microgels, we fluorescently labeled the entrapped oil droplets using a lipophilic carbocyanine dye, PKH26, which exhibits strong partitioning to the droplet interface. We employed an encoding strategy based on particle shape to denote key compositional differences among the particles used: disc-shaped

H. Z. An,[+] M. E. Helgeson,[+] Prof. P. S. Doyle
Massachusetts Institute of Technology
77 Massachusetts Avenue
Room 66-270, Cambridge, MA 02139, USA
E-mail: pdoyle@mit.edu
[+] These authors contributed equally to this work.

DOI: 10.1002/adma.201200214

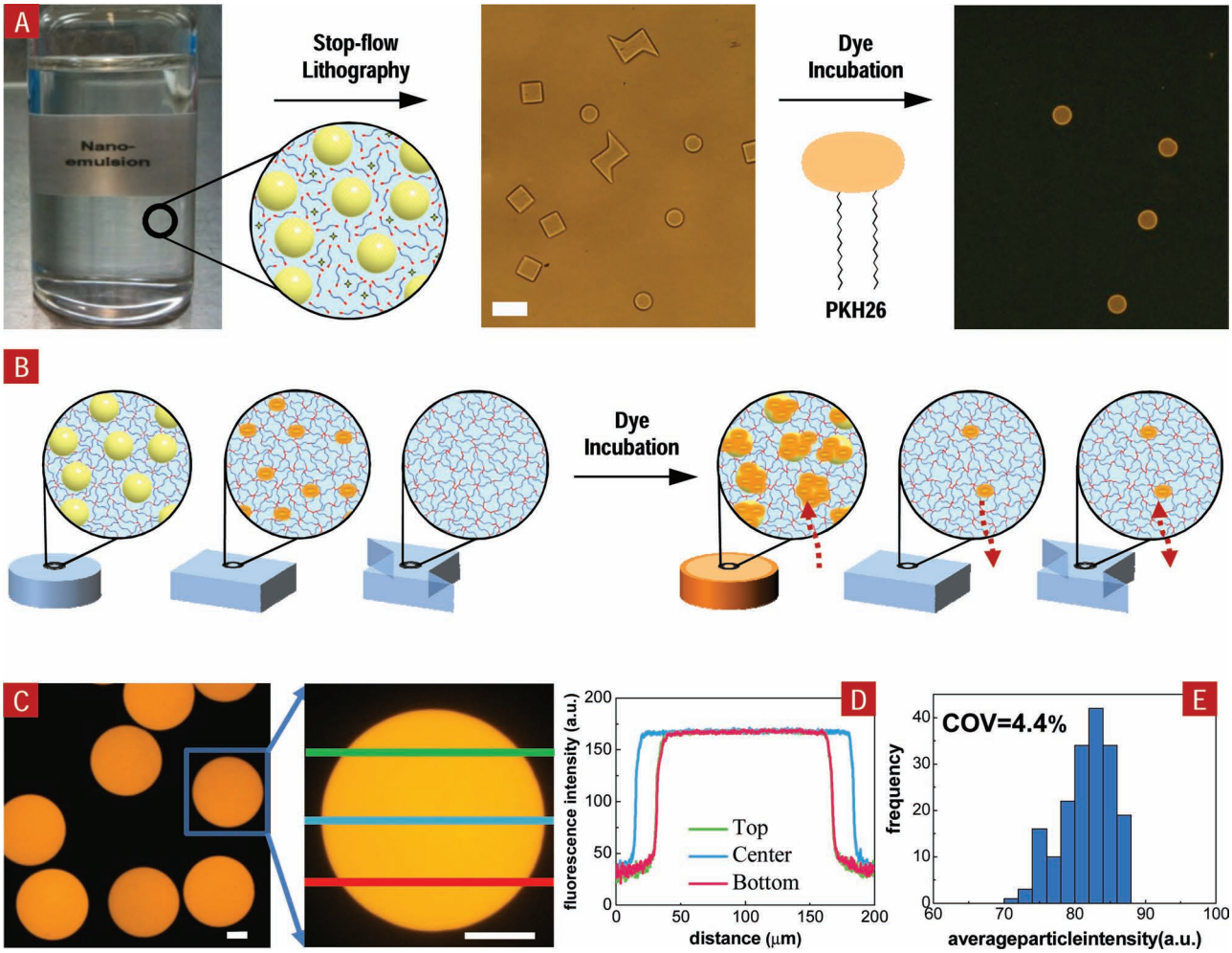

Figure 1. Schematic of nanoemulsion encapsulation and variation in loading of a model hydrophobe within microgel particles. (A) High pressure homogenization is used to produce optically-transparent, photo-crosslinkable O/PG nanoemulsions (left). Stop-flow lithography allows the nanoemulsion to be photo-patterned into microgel particles with controlled size and shape (center). Incubation of microgel particles with a hydrophobic dye (PKH26) demonstrates successful encapsulation of the nanoemulsion (right). (B) Schematic depiction of the particles shown in the micrographs in (A). As synthesized, the disc-shaped, square-shaped, and Z-shaped particles contain nanoemulsion without dye, dye without nanoemulsion, and neither dye nor nanoemulsion, respectively. Upon incubation with dye, dye is preferentially absorbed by the particles containing nanoemulsion, whereas it is not retained by particles without nanoemulsion. Arrows indicate the net flux of dye during incubation. (C) Fluorescent micrograph of monodisperse disc-shaped particles pre-loaded with PKH26. (D) Spatially resolved fluorescence intensity profiles (a.u. = arbitrary units) taken across three different regions of the particle shown in (C, right). (E) Statistical distribution of fluorescence intensities of the particles (N = 181) shown in (C). Fluorescence coefficient of variation (COV) is less than 4.4%. Scale bars are 50 μm.

particles initially contained nanoemulsions without PKH26, square-shaped particles contained PKH26 without nanoemulsion, and Z-shaped particles contained neither nanoemulsion nor PKH26. Upon PKH26 incubation, only disc-shaped particles exhibited fluorescence, demonstrating that PKH26 is preferentially loaded into the nanoemulsion droplets that are encapsulated within the hydrogel matrix (Figure 1A,B).

The demonstrated ability to confine nanoemulsions within a microgel can potentially be used to encapsulate hydrophobic active compounds. To test this hypothesis, we employ PKH26 as a model lipophilic active, where its fluorescence provides a convenient route for quantification of loading uniformity, the lack of which may reduce encapsulation efficiency and control over desired release characteristics. Here, PKH26 (5 μM) is incorporated directly into the O/PG pre-cursor, without any additional dye incubation. Figure 1C shows a typical collection of monodisperse disc-shaped particles synthesized using SFL. Photoluminescence analysis indicates highly uniform fluorescence both across different particles (Figure 1E) and within any given particle, where the fluorescence is uniform to sub-micron length scales (<400 nm) corresponding to the resolution of the 40× microscope objective (Figure 1D). To our knowledge, this high degree of homogenous and reproducible loading of the nanoemulsion, and consequently the active, outperforms commonly used particle synthesis techniques based on droplet microfluidics.[32,35]

The delivery of microparticle-based vehicles in vivo has been shown to depend strongly on particle shape.[36] As such, the ability of SFL to generate morphologically complex particles in a high-throughput fashion yields distinct advantages over other fluidic methods,[32,37] which are limited to production of spheroidal particles with limited chemical anisotropy. To show this, we have synthesized various composite microgels comprising polygonal solids (**Figure 2**A-C) with characteristic sizes ranging from 30 to 180 μm. All of the particles show fidelity to the original mask shape and are uniform with respect to size and fluorescence intensity. In addition to shape anisotropy, SFL can generate microgels with sophisticated chemical anisotropy.[24,25] To demonstrate this for our composite microgels, we created multifunctional particles having segregated compartments with different compositions or stored actives. In one case, Janus microgels were prepared by patterning tablet-shaped particles across the interface of two co-flowing pre-cursor streams, one with and one without PKH26-labeled nanoemulsion, resulting in confinement of the nanoemulsion to a distinct compartment (Figure 2D, inset). The sharp interface between the two halves of the particle persists for several days (Figure 2D), indicating negligible mobility of the encapsulated nanoemulsion droplets within the hydrogel matrix. In another case, a similar procedure was used to generate multifunctional dumbbell-shaped particles with five spatially alternating regions containing different active compounds, red fluorescent PKH26 and green fluorescent $DiO(C_{18})_2$ (Figure 2E). The resulting particles demonstrate minimal interpenetration between neighboring compartments (Figure 2F). In total, these studies demonstrate a high degree of compatibility of the O/PG nanoemulsions with the SFL process, and more complex composite microgels could easily be created by flowing or stacking more concurrent laminar streams containing functional and functionalizable materials.[26,27,29,38,39]

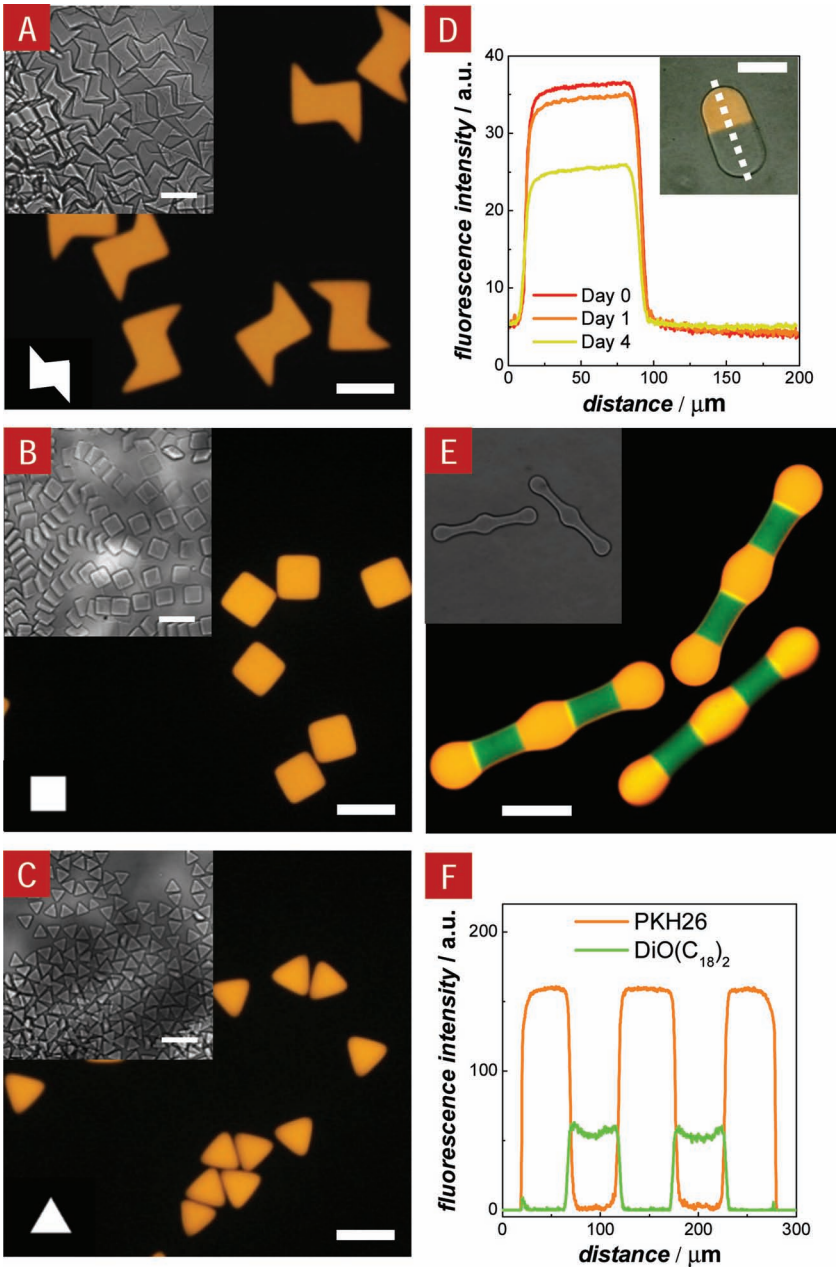

Figure 2. Geometrically and chemically complex nanoemulsion-laden particles synthesized using SFL. All particles are made using a 20X microscope objective. As synthesized, the Z-shaped (A), square-shaped (B), and triangle-shaped (C) particles have characteristic feature sizes of 70, 50, and 30 μm, respectively. (A)-(C) each shows fluorescent and bright-field (upper left inset) micrographs of a particle array and the corresponding transparency mask feature (lower left inset) used during synthesis. (D) Time evolution of fluorescence intensity scans along the long axis (dashed white line) of tablet-shaped Janus particles shown in upper right inset. These particles contain both nanoemulsion-laden (orange) and control (gray) sections. The enduring sharpness of the Janus interface suggests minimal migration of the nanoscopic compartments over time. (E) Overlaid fluorescent micrographs demonstrating the co-encapsulation of two different hydrophobic dyes in five distinct regions of dumbbell-shaped particles. (F) Spatially resolved intensity profiles of the orange (PKH26) and green ($DiO(C_{18})_2$) fluorescence in the multi-compartment particles shown in (E) demonstrate minimal interpenetration between neighboring compartments. Scale bars are 50 μm.

Having established the production of nanoemulsion-laden microgels by SFL, we sought to prove a number of different motifs for their use in controlled encapsulation and release of both hydrophobic and hydrophilic active compounds that take advantage of the homogeneous, nano-scale distribution of droplets within the particle. Specifically, we show how encapsulation can be achieved either through solubility within the oil phase, through molecular anchoring at the oil-water (O/W) interface, or through the release of the nanoemulsion droplets themselves in concert with these motifs.

The simplest method for encapsulation of hydrophobic species is solubility within the nanoemulsion. As already shown, loading of the microgels can be performed either before

particle synthesis by direct encapsulation or by thermodynamic partitioning. The former method enables localization of the active to various compartments within the particle (Figure 2E), whereas the latter enables differential loading based on incubation conditions (see Supporting Information). Release of solubilized actives from ordinary nanoemulsions typically occurs as a "burst" due to the high surface area of the droplets.[6] By contrast, solubility-based release from our composite microgel particles will be controlled by both the departure of the active from the O/W interface and subsequent diffusion through the crosslinked hydrogel.[3] This is demonstrated in **Figure 3**A, where release of PKH26 dye from composite microgels was monitored by quantifying the average particle fluorescence over time. As shown, the release of PKH26 is sustained over a period of multiple weeks, with a characteristic time scale of $\tau = 7.6$ days. This suggests that the release process is primarily limited by desorption of the active compound from the O/W interface. After a period of several weeks, the particles were re-incubated with an amount of PKH26 stoichiometrically equal to the initial concentration, after which the particles exhibited total recovery of their initial fluorescence. Thus, the nanoemulsion remains stably encapsulated within the microgel for long periods of time, enabling sustained release as well as reloading on demand. In concert with the Janus motifs shown previously, these principles could be used to design composite microgel particles with sophisticated release profiles, whereby the barrier to release can be varied in a controlled fashion by tuning rate of desorption through the materials and compositions comprising the O/PG nanoemulsion.

In order to extend the controlled encapsulation and release capabilities of our composite microgels to soluble bioactives, we used a generic scheme for the attachment of biomolecules based on previous work,[40] in which a biotinylated (BT) linker is incorporated into the composite microgels, and a streptavidin functionalized with cyanine dye (SA-Cy3) was used as a reporter and model soluble protein to be encapsulated. Because of the structure of the hydrogel-nanoemulsion composite scaffold, attachment of biotin moieties to the particle can be achieved through a number of mechanisms, which identify several potential motifs for encapsulation and release of bioactives. One motif involves covalent attachment of an acrylate-functionalized biotinylated nucleotide (Ac-BT) to the crosslinked hydrogel network via photopolymerization, which can then bind SA-Cy3 during post-processing to form an encapsulated BT-SA-Cy3 complex. Though this scheme has been previously demonstrated,[40] we found that it is not compromised by the presence of encapsulated nanoemulsions (see Supporting Information).

Another possible motif involves functionalization of the bioactive with a hydrophobe, enabling encapsulation within composite microgels by amphiphilic anchoring at the surface of the nanoemulsion droplets. In previous work, we showed encapsulation and triggered release of BT-SA-Cy3 through strong irreversible hydrophobic anchoring to the O/W interface using a photolabile cholesterol linker.[18] Here, we explore an alternative mechanism of reversible anchoring, which is controlled by the relative strength of adsorption of the hydrophobe, and can thus be triggered by changes in solution conditions (Figure 3B). To demonstrate this, we utilize our previous observation that acrylic moieties exhibit temperature-induced partitioning at the

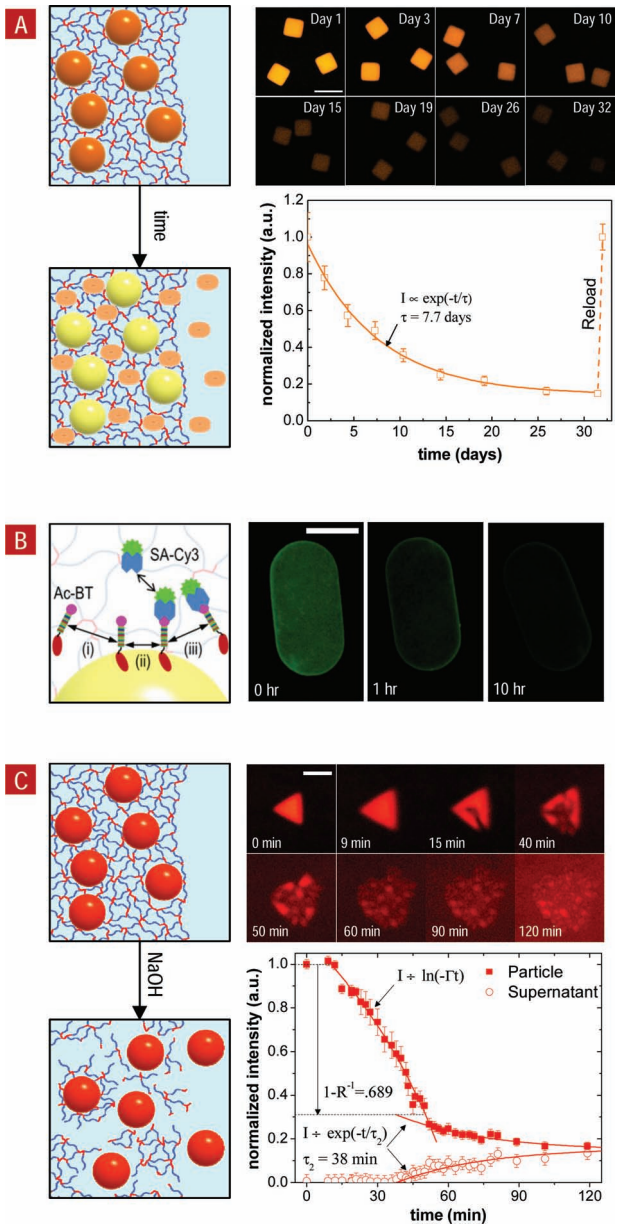

Figure 3. Several methods for controlled encapsulation and release of small molecules, biomolecules and nanoemulsion droplets from composite microgels: left–schematic molecular workflow diagrams, right–color fluorescence micrographs of representative microgel particles (scale bars are 100 µm) and photoluminescence analysis (where appropriate). (A) Encapsulation of PKH26 within the nanoemulsion and subsequent sustained release due to limited solubility in the solution phase. Micrographs show elution of the active into dye-free buffer over a period of several weeks, with first- order release kinetics. The depleted particles can be stoichiometrically reloaded with dye (dotted orange line). (B) Encapsulation and release by reversible hydrophobic anchoring to the nanoemulsion O-W interface. (i) Particles are incubated at 45 °C with Ac-BT, which partition to the O-W interface, and (ii) monitored by SA-Cy3 reporter. (iii) A decrease in temperature to 15 °C results in release of the Ac-BT-SA-Cy3 complex from the O-W interface. Micrographs show subsequent release of the reporter over several hours (color-enhanced to show detail). (C) Release of nanoemulsion droplets by degradation of the hydrogel matrix. Saponification at high pH first results in swelling of the particle at short times, followed by degradation of the particle and release of the nanoemulsion over a period of hours.

O/W interface.[18] "Empty" tablet-shaped microgels containing nanoemulsion but no active were incubated with Ac-BT at 45 °C to induce anchoring of the acrylic groups to the nanoemulsion droplets. After incubation with SA-Cy3 reporter, the particles exhibited significant fluorescence (Figure 3B), demonstrating controlled encapsulation of SA-Cy3. Upon cooling the microgel suspension to 15 °C, particles then exhibited a significant decrease in fluorescence over a period of hours, indicating desorption of acrylic groups from the O/W interface and subsequent release of the Ac-BT-SA-Cy3 complex.

Finally, we demonstrate a highly orthogonal motif of delivery by release of the nanoemulsion droplets themselves from the composite microgel particles. For our PEG hydrogels, we achieve this through saponification and subsequent physical degradation of the hydrogel matrix by incubating the particles under basic pH conditions (Figure 3C). Triangle-shaped particles were synthesized using a nanoemulsion containing the hydrophobic dye Nile Red, resulting in composite microgels with initially uniform loading. Upon transfer into high pH buffer, the particles degrade over time with two qualitatively different kinetic regimes identified by photoluminescence analysis. In the first regime, the particles swell appreciably over a period of 60 minutes. Initially, this swelling is uniform and isotropic, whereas at long times dark-colored fractures develop in the particle surface (see Supporting Information for corresponding bright-field images). Over this time, we observe a significant decrease in particle fluorescence that is logarithmic in time such that $I/I_0 \sim \ln(-\Gamma t)$, where $\Gamma = 2.0\ s^{-1}$ is a characteristic rate of swelling. We note that the decrease in fluorescence intensity over this period is entirely accounted for by the volumetric swelling of the particle (characterized by a swelling ratio $R = 3.21$, such that $1\text{-}R^{-1} = 0.689$ coincides with the loss of particle fluorescence over this period). Since the supernatant phase exhibits no observable fluorescence over this period, we conclude that the initial decrease in intensity is due entirely to swelling of the particle, and not from release of the nanoemulsion droplets. At long times (>40 min), a qualitatively different behavior is observed in which the particle exhibits no additional swelling, and the particle fluorescence decreases over time while that of the supernatant phase increases at a similar rate. We find that both the decrease in particle fluorescence and increase in supernatant fluorescence can be quantitatively described by a single characteristic time of $\tau = 38$ min. As such, the observed changes in fluorescence at long times are due primarily to the release of nanoemulsion droplets liberated by degradation of the hydrogel matrix.

These results suggest the following mechanism of release of the nanoemulsion droplets during degradation of the PEGDA matrix (Figure 3C). Saponification causes cleavage of acrylic esters within the crosslinked PEGDA network, which decreases the crosslink density of the hydrogel matrix over time. Initially, this decrease is sufficient to give rise to significant swelling of the particle,[41] but still mild enough that the droplets remain sterically trapped within the polymer network. However, after a critical time, the hydrogel network is ultimately degraded to a point where the mesh size of the hydrogel increases beyond the size of the droplets, at which point they can freely diffuse throughout the particle and into the supernatant. Assuming that pH equilibration and saponification within the particle are not diffusion-limited, this critical time is homogeneous throughout the particle, and release of the nanoemulsion droplets thus follows simple first-order kinetics corresponding to diffusion of the droplets from the particle interior into a semi-infinite supernatant medium.

In summary, we have shown that the combination of O/PG nanoemulsions and SFL presents a versatile new material platform for producing shape- and chemically-anisotropic designer hydrogels containing nanoscopic hydrophobic compartments of controlled size and loading. These properties have allowed us to develop a suite of capabilities (solubilization, covalent conjugation, hydrophobic anchoring, and matrix degradation) for encapsulation and release of model compounds via orthogonal methods *from a single particle*. In particular, the O/W interface presents a novel means of hydrogel encapsulation, whereby hydrophobic anchoring can be used to achieve both sustained and triggered release. Furthermore, matrix degradation allows for liberation of the nanoemulsion droplets as nanoparticle vehicles for further transport and delivery of actives. The measured release kinetics cover time scales ranging from an hour to several weeks depending on the release mechanism, providing a highly flexible system for material formulation and design. Compatible actives include both hydrophobic and hydrophilic species, and span a broad class of small molecules and biologics.

These results hold significant potential for the development of new systems for controlled encapsulation and release. The nanoemulsion loadings achieved in our composite microgels have, to our knowledge, among the highest hydrophobic loading capacities ever demonstrated in a hydrogel material. Moreover, the liquid droplets could be used as nanoscopic reactors for non-polar chemistries. Finally, the composite microgels lend themselves to novel encapsulation and release strategies. For example, hierarchical delivery could be achieved by administration of the microgel as a concentrated package of nanoemulsion cargo, from which the droplets can be deployed by matrix degradation, thereby making them available as nanocarriers to potentially couple with targeted delivery strategies[42–44] using molecular motifs such as hydrophobic anchoring. As such, further studies of these materials involving extension of actives used to more relevant therapeutics and nutrients, as well as rational control of the particle microstructure to tune release kinetics, will test their suitability in a wide range of applications including pharmaceuticals, multi-drug therapies, consumer products, and foods.

Experimental Section

Materials and Nanoemulsion Preparation: The oil-in-pregel nanoemulsions (O/PG) used in this work contain silicone oil (Dow Corning, viscosity ~ 5 cP) dispersed in an aqueous phase consisting of poly(ethylene glycol) diacrylate (PEGDA, $M_n = 700\ g\ mol^{-1}$) and sodium dodecyl sulfate (SDS). Additives included the photoinitiator 2-hydroxy-2-methyl-1-phenyl-propan-1-one (Darocur 1173) and 1 mM solutions of lipophilic dyes, PKH26 ($\lambda_{ex}/\lambda_{em}$ = 551/567 nm), Nile Red ($\lambda_{ex}/\lambda_{em}$ = 550/626 nm) and 3,3'-dioctadecyloxacarbocyanine perchlorate ($DiO(C_{18})_2$, $\lambda_{ex}/\lambda_{em}$ = 484/501 nm, Invitrogen) in ethanol were used to fluorescently label the oil nanodroplets. Unless otherwise noted, all materials were obtained from Sigma Aldrich and used as supplied.

To prepare the photo-crosslinkable nanoemulsions, a crude pre-emulsion was first generated as previously described[18] by adding silicone

oil drop-wise to a pre-mixed aqueous continuous phase containing 33% (v/v) PEGDA and 100 mM SDS under constant agitation using a magnetic stirrer. The corresponding nanoemulsion was then created by high pressure homogenization (EmulsiFlex-C3, AVESTIN) at 15 kpsi for 16 passes, with cooling in between passes to 4 °C. Dynamic light scattering measurements (BI200-SM, Brookhaven Instruments) indicate the as-prepared nanoemulsion had an average droplet diameter, $\langle D \rangle$, of 45 nm (Figure S1). 2% (v/v) Darocur 1173 and 5-10 μM lipophilic dyes (as necessary) were added to aliquots of nanoemulsion, followed by vortex mixing. The resulting fluid was passed through a 25 mm Acrodisc syringe filter (0.45 μm Supor Memberane, Pall Corporation) to eliminate any coalesced droplets, and finally stored at 4 °C until further use.

Particle Synthesis: All of the particles shown in this work were prepared using stop-flow lithography as described previously[45,46] in multi-inlet (up to six inlet ports) rectangular microfluidic channels (PDMS, Sylgard 184, Dow Corning). Briefly, the pre-cursor mixture was injected into a synthesis device using modified pipette tips (Molecular BioProducts) as delivery chambers under moderate forcing pressure (~3 psi). Composite microparticles were patterned by projecting mask-defined UV light from a Lumen 200 metal arc lamp (Prior Scientific) through a wide excitation UV filter set (11000v2 UV, Chroma Technology). A shutter system (VS25, Uniblitz) interfaced with a custom-written Python automation script precisely controls the duration of UV exposure, which typically ranged from 150 to 800 ms depending on particle shape and size. The formation of the microparticles was visualized using a cooled interline charge-coupled device camera (Clara, Andor).

Following polymerization, particles were transferred from the outlet reservoir of the synthesis microfluidic device to a clean 1.5 mL Eppendorf tube containing 300 μL PBST (1X phosphate buffered saline with 0.5% (v/v) Tween 20 (Sigma-Aldrich). Particles were washed and re-suspended at least four times via centrifugal separation followed by decanting and replacement of the supernatant, and subsequently stored at room temperature for imaging.

Particle Characterization and Photoluminescence Analysis: Droplets of samples containing up to 100 fluorescently labeled particles were transferred onto a glass slide and visualized by bright-field and fluorescence optical microscopy using long-pass filter sets (XF101-2 for PKH26, Cy3 and Nile Red, XF100-2 for DiO$(C_{18})_2$, Omega Optical). High resolution fluorescent images of the particles were captured with a digital SLR camera (D200, Nikon) and processed using NIH ImageJ software to obtain size and fluorescence intensity data. For all measurements, images of at least 10 particles were taken in order to obtain sufficient statistical information. Care was taken to standardize the experimental conditions (e.g., camera exposure time, lamp intensity setting, microscope objective, etc.) used in imaging studies. Prior to each imaging session, the lamp intensity was calibrated with a power meter (Model 1815-C, Newport).

Dye Encapsulation and Release Studies: For solubility-based release assays, square-shaped particles were synthesized from an O/PG nanoemulsion containing 5 μM PKH26 dye and purified into 1x PBST buffer. Fluorescence imaging and subsequent photoluminescence analysis was then used to monitor the particle fluorescence over time for a period of several weeks. Particles were stored and imaged at 23 °C. Square-shaped particles depleted of PKH26 (after about 5 weeks of sustained release) were incubated with dye overnight at 35 °C and 1500 rpm (H5000-HC, Biomega). To achieve dye reloading, the particle concentration in the remaining suspension was then estimated by image analysis (using bright-field imaging). The resulting concentration was used to estimate the concentration of PKH26 at which stoichiometric re-loading of the dye would be achieved relative to the initial dye concentration during synthesis. The particles were then washed in PBST buffer containing the estimated PKH26 concentration. After incubation, the particles were washed four times in neat PBST buffer and imaged under the same conditions as those used throughout the protracted study of dye release.

For protein conjugate encapsulation and release studies, we used a generic fluorescent streptavidin-biotin (SA-BT) reporter complex[40] as a model biomolecular cargo, which was encapsulated through several orthogonal motifs. An acrylate-modified biotinylated peptide (Ac-BT) was obtained from Integrated DNA Technologies, and a 0.5 mM stock was prepared in TET (1X Tris-EDTA (TE) with 0.5% (v/v) Tween 20) buffer. A fluorescent cyanine-conjugated streptavidin reporter (SA-Cy3) was obtained from Sigma Aldrich, and a 1 mM stock was prepared in 1x TET buffer. For encapsulation by covalent attachment to the hydrogel matrix, see Supporting Information for details.

For encapsulation and release by reversible hydrophobic anchoring, tablet-shaped particles were synthesized from a non-fluorescent O/PG nanoemulsion ($\varphi = 0.20$) and purified into TET buffer. Aliquots of the particle suspension were then transferred into a 5.0 μM Ac-BT solution in TET buffer at a concentration of ~1 particle/μL and incubated overnight on a shaker plate at 45 °C and 1500 rpm. The elevated temperature during incubation drives the partitioning of the weakly hydrophobic acrylate pendant groups to the oil-water interface.[18] The particles were then washed with neat TET at 45 °C to remove excess Ac-BT in the supernatant, and subsequently centrifuged and re-suspended in 3.5 μM SA-Cy3 to initiate formation of Ac-BT-SA-Cy3 complex. The suspension was then placed on a shaker plate at 45 °C and 1500 rpm for 4 hours, and then washed with neat TET buffer at 45 °C to remove excess SA-Cy3. Aliquots of the resulting suspension were then prepared on microscope slides and imaged using a temperature-controlled microscope stage (TSA02i, Instec Inc.). Particles were first imaged at 45 °C to confirm encapsulation of Ac-BT-SA-Cy3 by hydrophobic anchoring using photoluminescence analysis. Subsequently, the temperature was quickly decreased to 15 °C, and images were taken over time to observe changes in particle fluorescence using photoluminescence analysis.

Particle Degradation Studies: To demonstrate release of the fluorescently labeled nanoemulsions via saponification and subsequent PEGDA hydrogel degradation, triangle-shaped particles were synthesized using an O/PG nanoemulsion containing 10 μM Nile Red dye ($\varphi = 0.33$, $P = 0.33$, $C_s = 100$ mM, $I = 0.02$). The particles were purified and imaged in PBST buffer. Subsequently, particles were separated by centrifugation and re-suspended in 0.1 M NaOH in PBST buffer. The particles were then imaged over time in both bright-field and fluorescence mode. The bright-field counterparts for the time-lapsed fluorescent images shown in Figure 3C in the main text appear in Figure S4.

Supporting Information

Supporting Information is available from the Wiley Online Library or from the author.

Acknowledgements

MEH acknowledges support from the Novartis-MIT Center for Continuous Manufacturing. Additional support is provided by the Institute for Collaborative Biotechnologies through grant W911NF-09-0001 from the U. S. Army Research Office and National Science Foundation grants CMMI-1120724 and DMR-1006147. The content of the information does not necessarily reflect the position or the policy of the Government, and no official endorsement should be inferred. HZA and MEH thank S. C. Chapin, P. Panda, and R. Srinivas for helpful discussions.

Received: January 15, 2012
Published online: March 26, 2012

[1] N. A. Peppas, P. Bures, W. Leobandung, H. Ichikawa, *Eur. J. Pharm. Biopharm.* **2000**, *50*, 27.
[2] A. S. Hoffman, *Adv. Drug Deliv. Rev.* **2002**, *54*, 3.
[3] T. R. Hoare, D. S. Kohane, *Polymer* **2008**, *49*, 1993.

[4] N. Kolishetti, S. Dhar, P. M. Valencia, L. Q. Lin, R. Karnik, S. J. Lippard, R. Langer, O. C. Farokhzad, *Proc. Nat. Acad. Sci. USA* **2010**, *107*, 17939.
[5] C. C. Muller-Goymann, *Eur. J. Pharm. Biopharm.* **2004**, *58*, 343.
[6] D. J. McClements, *Soft Matter* **2011**, *7*, 2297.
[7] O. Couture, M. Faivre, N. Pannacci, A. Babataheri, V. Servois, P. Tabeling, M. Tanter, *Med. Phys.* **2011**, *38*, 1116.
[8] D. C. Pregibon, M. Toner, P. S. Doyle, *Science* **2007**, *315*, 1393.
[9] B. Jeong, Y. H. Bae, S. W. Kim, *J. Controlled Release* **2000**, *63*, 155.
[10] R. Langer, D. A. Tirrell, *Nature* **2004**, *428*, 487.
[11] V. Jenning, A. Gysler, M. Schafer-Korting, S. H. Gohla, *Eur. J. Pharm. Biopharm.* **2000**, *49*, 211.
[12] P. C. Chen, D. S. Kohane, Y. J. Park, R. H. Bartlett, R. Langer, V. C. Yang, *J. Biomed. Mater. Res., Part A* **2004**, *70A*, 459.
[13] M. L. Gou, X. Y. Li, M. Dai, C. Y. Gong, X. H. Wang, Y. Xie, H. X. Deng, L. J. Chen, X. Zhao, Z. Y. Qian, Y. Q. Wei, *Int. J. Pharm.* **2008**, *359*, 228.
[14] D. Gulsen, C. C. Li, A. Chauhan, *Curr. Eye Res.* **2005**, *30*, 1071.
[15] H. Yan, K. Tsujii, *Colloids Surf., B* **2005**, *46*, 142.
[16] Y. Lapitsky, E. W. Kaler, *Soft Matter* **2006**, *2*, 779.
[17] D. Gulsen, A. Chauhan, *Int. J. Pharm.* **2005**, *292*, 95.
[18] M. E. Helgeson, S. E. Moran, H. Z. An, P. S. Doyle, *Nat. Mater.* **2012**, DOI:10.1038/nmat3248.
[19] D. J. McClements, in *Annual Review of Food Science and Technology*, Vol. *1* (Eds: M. P. Doyle, T. R. Klaenhammer), **2010**, 241.
[20] T. G. Mason, J. N. Wilking, K. Meleson, C. B. Chang, S. M. Graves, *J. Phys.: Condens. Matter* **2006**, *18*, R635.
[21] Y. Geng, D. E. Discher, *Polymer* **2006**, *47*, 2519.
[22] B. M. Discher, D. A. Hammer, F. S. Bates, D. E. Discher, *Curr. Opin. Colloid Interface Sci.* **2000**, *5*, 125.
[23] J. C. Brackman, J. Engberts, *Chem. Soc. Rev.* **1993**, *22*, 85.
[24] D. Dendukuri, P. S. Doyle, *Adv. Mater.* **2009**, *21*, 4071.
[25] M. E. Helgeson, S. C. Chapin, P. S. Doyle, *Curr. Opin. Colloid Interface Sci.* **2011**, *16*, 106.
[26] K. W. Bong, K. T. Bong, D. C. Pregibon, P. S. Doyle, *Angew. Chem. Int. Ed.* **2010**, *49*, 87.
[27] K. W. Bong, D. C. Pregibon, P. S. Doyle, *Lab Chip* **2009**, *9*, 863.
[28] D. C. Appleyard, S. C. Chapin, P. S. Doyle, *Anal. Chem.* **2011**, *83*, 193.
[29] D. K. Hwang, J. Oakey, M. Toner, J. A. Arthur, K. S. Anseth, S. Lee, A. Zeiger, K. J. Van Vliet, P. S. Doyle, *J. Am. Chem. Soc.* **2009**, *131*, 4499.
[30] S.-H. Kim, H. C. Shum, J. W. Kim, J.-C. Cho, D. A. Weitz, *J. Am. Chem. Soc.* **2011**, *133*, 15165.
[31] B. J. Sun, H. C. Shum, C. Holtze, D. A. Weitz, *ACS Appl. Mater. Interfaces* **2010**, *2*, 3411.
[32] D. Jagadeesan, I. Nasimova, I. Gourevich, S. Starodubtsev, E. Kumacheva, *Macromol. Biosci.* **2011**, *11*, 889.
[33] S. H. Kim, J. W. Shim, S. M. Yang, *Angew. Chem. Int. Ed.* **2011**, *50*, 1171.
[34] S. Mitragotri, J. Lahann, *Nat. Mater.* **2009**, *8*, 15.
[35] Y. Zhao, H. C. Shum, H. Chen, L. L. A. Adams, Z. Gu, D. A. Weitz, *J. Am. Chem. Soc.* **2011**, *133*, 8790.
[36] J. A. Champion, Y. K. Katare, S. Mitragotri, *J. Controlled Release* **2007**, *121*, 3.
[37] H. C. Shum, Y.-j. Zhao, S.-H. Kim, D. A. Weitz, *Angew. Chem. Int. Ed.* **2011**, *50*, 1648.
[38] J. H. Jang, D. Dendukuri, T. A. Hatton, E. L. Thomas, P. S. Doyle, *Angew. Chem. Int. Ed.* **2007**, *46*, 9027.
[39] R. F. Shepherd, P. Panda, Z. Bao, K. H. Sandhage, T. A. Hatton, J. A. Lewis, P. S. Doyle, *Adv. Mater.* **2008**, *20*, 4734.
[40] S. C. Chapin, D. C. Appleyard, D. C. Pregibon, P. S. Doyle, *Angew. Chem. Int. Ed.* **2011**, *50*, 2289.
[41] N. A. Peppas, J. Z. Hilt, A. Khademhosseini, R. Langer, *Adv. Mater.* **2006**, *18*, 1345.
[42] M. E. Davis, Z. Chen, D. M. Shin, *Nat. Rev. Drug Discovery* **2008**, *7*, 771.
[43] S. M. Nie, Y. Xing, G. J. Kim, J. W. Simons, in *Annual Review of Biomedical Engineering*, Vol. *9*, **2007**, 257.
[44] L. Brannon-Peppas, J. O. Blanchette, *Adv. Drug Deliv. Rev.* **2004**, *56*, 1649.
[45] D. Dendukuri, D. C. Pregibon, J. Collins, T. A. Hatton, P. S. Doyle, *Nat. Mater.* **2006**, *5*, 365.
[46] D. Dendukuri, S. S. Gu, D. C. Pregibon, T. A. Hatton, P. S. Doyle, *Lab Chip* **2007**, *7*, 818.